High refractive index low-loss aluminium oxide waveguides

(Student Paper)

W.A.P.M. Hendriks, M. Dijkstra, C.I. van Emmerik, I. Hegeman S.M. García-Blanco
MESA+ Institute, University of Twente, P.O. Box 217, 7550 AE, Enschede, The Netherlands
e-mail: w.a.p.m.hendriks@utwente.nl

ABSTRACT

A high refractive index (n~1.715 at 633 nm of wavelength) aluminium oxide slab waveguide has been developed, which exhibits very low losses from the near-UV to the near infrared wavelength range. Slab waveguide losses as low as 1.8 dB/cm at 407 nm and less than 0.1 dB/cm at 1550 nm of wavelength have been experimentally characterized. Such low losses are limited by surface scattering. The layer was deposited by reactive sputter coating with an aluminium target, a set substrate temperature of 700 C and an oxidation state of the target of 5 %. The very high optical quality of this material, in combination with rare-earth ion doping, could pave the way towards high-gain on-chip amplifiers in different wavelength ranges, on-chip lasers and non-linear applications.

Keywords: Aluminium oxide, refractive index, low loss, sputtering.

1. INTRODUCTION

The excellent optical properties of aluminium oxide (Al_2O_3) make it a very interesting material for integrated photonics[1]–[4]. The large transparency window from 150 nm up to 5500 nm allows for applications from the UV to the mid-infrared [5]. Rare earth ion doped amplifiers and lasers have been shown in amorphous aluminium oxide with wavelengths ranging from 880 nm to up to 2 µm [4], [6]–[8]. Integration with passive photonic platforms has been the subject of much research efforts recently [7], [9]–[12].

Reactive sputter deposition can be utilized to deposit high optical quality thin films for integrated optical circuits with reasonably high deposition rates. The potential of reactive sputter coating of optical grade amorphous Al_2O_3, has previously been demonstrated by Wörhoff et al. [13], where they optimized the sputter coating process to achieve a propagation loss of 0.3 and 0.1 dB/cm at a wavelength of 633 nm and 1550 nm respectively for a low refractive index material (n~1.65 at 633 nm). Low losses were achieved by optimizing the process over a large parameter space. Substrate temperature was reported as the main parameter that influences propagation loss. They also compared DC and RF sputter coating, the latter delivering higher layer quality, most likely due to reduced arcing during the process.

Similar propagation losses were obtained by Magden et al. [14] for an optimized process with the addition of a bias voltage to the substrate. The deposited material also exhibited a low refractive index (n~1.578 at 1550 nm).

In this work, an Al_2O_3 layer with high refractive index (i.e., n~1.715 at 633 nm) is deposited by increasing the set temperature of the substrate during sputtering to 700 ºC. Very low slab losses of ~1.8 dB/cm at 407 nm and well below 0.1 dB/cm at 1550 nm were experimentally demonstrated in this high refractive index Al_2O_3 layer.

2. DEPOSITION AND CHARACTERIZATION OF ALUMINIUM OXIDE THIN FILMS

The Al_2O_3 layers were deposited using an AJA ATC 15000 RF reactive co-sputtering system [13] on 10 cm diameter silicon wafers with 8 µm thick thermal oxide. The system can host three 2 inch RF guns, one of which was installed with an aluminium target (Al, 99.9995 % purity). The main deposition chamber is evacuated to a base pressure of 0.1 µTorr (i.e., 13 µPa) to prevent incorporation of hydroxide ions in the layer, which induce absorption losses around 750 nm, 970 nm, and 1400 nm [15], and when the layer is doped with rare-earth ions, induce luminescence quenching [16]. The depositions are performed with a constant RF power of 200 W applied to the aluminium target. Before the start of the process, the bias voltage of the target as a function of oxygen flow into the chamber is measured. For low oxygen flows, the target is still mostly metallic. As the oxygen flow increases, the target starts oxidizing. Since the secondary electron emission yield of Al_2O_3 is higher than that of aluminium, the voltage drops to a minimum value that corresponds to a fully oxidized target [17]–[19]. A relatively low sputter flux combined with a large pump flux ensure that the bias curve evolves smoothly for our process[20]. The oxidation state of the target can be defined as

$$\eta_{ox} \equiv \frac{V_m - V_{O_2}}{V_m - V_{ox}} \qquad (1)$$

where V_m and V_{O_2} are the cathode bias voltage for a fully metallic target and a fully oxidized target surface respectively and V_{ox} is the bias voltage corresponding to the oxygen flow giving a relative oxidation state, η_{ox}. The relative oxidation state is used to compensate for the target erosion, which results in a changing bias curve,

changing deposition rate and a change in the ad-particle energy. Using the oxidation state of the target method allows us to reproduce layers over most of the target lifetime. In this work, an oxidation state of the target of 5% was selected, since this value resulted in low loss amorphous low refractive index (n~1.65) Al_2O_3 when the depositions were carried out at a set substrate temperature of 580 ºC. All parameters used for the deposition of the high index layer at 700 ºC are given in Table 1.

Table 1 Optimized Rf reactive sputtering process parameters

Parameter	**Value**	**Unit**
Argon flow	30	sccm
Oxygen flow	1.1	sccm
Relative bias voltage	5	%
Pressure	3.4	mTorr
Substrate set temperature	700	ºC
Target-substrate distance	15.2	cm
Power	200	W

The refractive index, thickness and propagation loss of the layer were measured using a Metricon 2010/M prism coupler instrument with a propagation loss module. The measurements were carried out at 407 nm, 474 nm, 532 nm, 632.8 nm, 827 nm, 983 nm, 1312 nm and 1550 nm [21]. The refractive index results are presented in Figure 1*A*, showing a refractive index increase of circa 0.05 compared to those obtained by Wörhoff et al. [13]. The increased index of refraction likely indicates an increased density of the layer. An increased layer density can reduce scattering from micro-voids and other growth defects in the layer due to a lower chance of occurrence as a result of the increased ad-particle mobility [22], [23]. Figure 1B shows the slab propagation loss as a function of wavelength. As it can be seen, a very low propagation loss of 0.025 dB/cm at 1550 nm was achieved, which is below the resolution of the measuring system. Propagation losses of 1.8 dB/cm at 407 nm are similar to the losses recently reported for low refractive index Al_2O_3 deposited by atomic layer deposition (ALD) [24]. The traced line in Figure 1B represents the Rayleigh scattering relation, given by the following equation,

$$\alpha(\lambda) = \alpha_0 \left(\frac{\lambda_0}{\lambda}\right)^4 \qquad (2)$$

where α_0 indicates the measured propagation loss at λ_0. The loss value at 632.8 nm was used to create the given curve. The excellent correspondence of the line trace suggests that the main contributor to the increased losses in the visible and near-UV is volume and surface scattering in the layer. Atomic force microscopy measurements show a surface roughness of the layer of 2.4 nm rms, which corresponds to the value calculated from the measured losses, which gives an expected surface roughness of 2.8 ±0.7 nm rms[25]

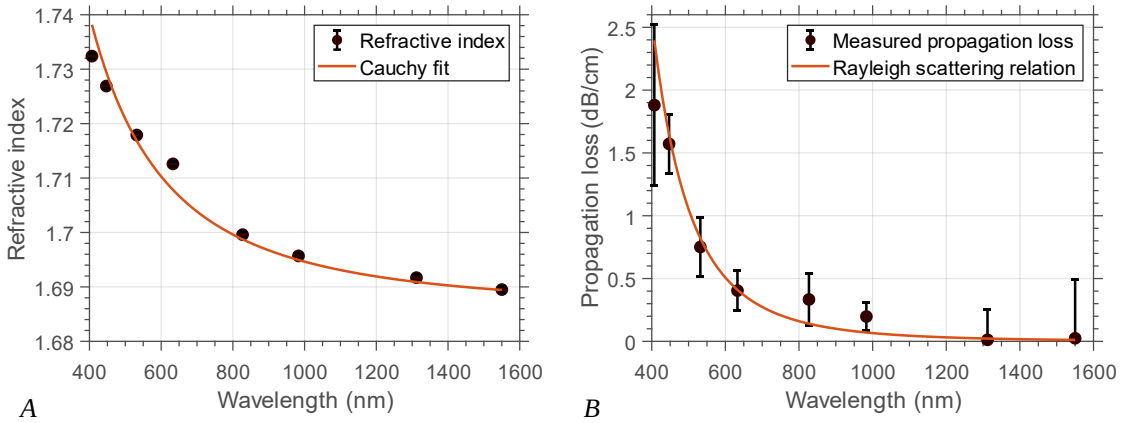

Figure 1 (A) Refractive index values (error +/-0.0005), with a Cauchy fit (coefficients: B=1.6852 and C=0.00899 µm²) (B) Propagation loss as a function of wavelength. fitted with the Rayleigh scattering relation indicating the loss mechanism of the layer is scattering dominated.

3. CONCLUSIONS

The development of high refractive index Al_2O_3 layer with low propagation loss from the near-UV to the mid-IR is very promising for integrated photonics in wavelength ranges where other materials do not perform. The increased refractive index of the layer allows for increased mode confinement. Finally, as the density increase is caused by a substrate temperature increase. It is possible that the layers exhibit a polycrystalline structure corresponding to a layer morphology of zone T or 2 [22], which needs to be further investigated. Polycrystallinity

might allow for increased rare earth ion dopant concentrations, where concentration quenching is prevented by a crystal lattice enforced inter-atomic distance of the dopant.

ACKNOWLEDGEMENTS

We would like to acknowledge John Jackson from Metricon for performing the refractive index and slab propagation loss measurements. Mike Dikkers, from the Mesa+ Nanolab, is acknowledge for useful discussions.

FUNDING

This work has been funded by the Dutch Research Council (NWO), under project number 15360.

REFERENCES

[1] J. D. Bradley *et al.*, "Integrated Al_2O_3:Er^{3+} ring lasers on silicon with wide wavelength selectivity," *Opt. Lett.*, vol. 35, no. 1, p. 73, 2010.

[2] L. Agazzi *et al.*, "Monolithic integration of erbium-doped amplifiers with silicon-on-insulator waveguides," *Opt. Express*, vol. 18, no. 26, p. 27703, 2010.

[3] S. a Vázquez-Córdova *et al.*, "Erbium-doped spiral amplifiers with 20 dB of net gain on silicon.," *Opt. Express*, vol. 22, no. 21, pp. 25993–6004, 2014.

[4] N. Li *et al.*, "Broadband 2-μm emission on silicon chips: monolithically integrated Holmium lasers," *Opt. Express*, vol. 26, no. 3, p. 2220, 2018.

[5] E. R. Dobrovinskaya *et al.*, "Application of Sapphire," in *Sapphire*, Boston, MA: Springer US, 2009, pp. 1–54.

[6] J. Yang *et al.*, "High-gain Al_2O_3:Nd^{3+} channel waveguide amplifiers at 880 nm, 1060 nm, and 1330 nm," *Appl. Phys. B Lasers Opt.*, vol. 101, no. 1–2, pp. 119–127, 2010.

[7] J. D. B. Bradley *et al.*, "Monolithic erbium- and ytterbium-doped microring lasers on silicon chips," *Opt. Express*, vol. 22, no. 10, p. 12226, 2014.

[8] J. D. B. Bradley *et al.*, "1.8-μm thulium microlasers integrated on silicon," 2016, p. 97440U.

[9] C. I. van Emmerik *et al.*, "Single-layer active-passive Al_2O_3 photonic integration platform," *Opt. Mater. Express*, vol. 8, no. 10, p. 3049, 2018.

[10] J. Mu *et al.*, "Resonant Coupling for Active-Passive Monolithic Integration of Al_2O_3 and Si_3N_4," *IEEE Photonics Technol. Lett.*, vol. 31, no. 10, pp. 771–774, 2019.

[11] J. Sun *et al.*, "Uniformly spaced λ/4-shifted Bragg grating array with wafer-scale CMOS-compatible process," *Opt. Lett.*, vol. 38, no. 20, p. 4002, 2013.

[12] M. Belt and D. J. Blumenthal, "Erbium-doped waveguide DBR and DFB laser arrays integrated within an ultra-low-loss Si_3N_4 platform," *Opt. Express*, vol. 22, no. 9, p. 10655, 2014.

[13] K. Wörhoff *et al.*, "Reliable Low-Cost Fabrication of Low-Loss Al_2O_3:Er^{3+} Waveguides With 5.4-dB Optical Gain," *IEEE J. Quantum Electron.*, vol. 45, no. 5, pp. 454–461, 2009.

[14] E. S. Magden *et al.*, "Monolithically-integrated distributed feedback laser compatible with CMOS processing," *Opt. Express*, vol. 25, no. 15, p. 18058, 2017.

[15] M. H. Weik and M. H. Weik, "hydroxyl ion overtone absorption," in *Computer Science and Communications Dictionary*, Springer US, 2000, pp. 742–742.

[16] L. Agazzi *et al.*, "Impact of luminescence quenching on relaxation-oscillation frequency in solid-state lasers," *Appl. Phys. Lett.*, vol. 100, no. 1, p. 011109, 2012.

[17] D. Depla *et al.*, "Influence of the target composition on the discharge voltage during magnetron sputtering," *Surf. Coatings Technol.*, vol. 201, no. 3–4, pp. 848–854, 2006.

[18] K. Strijckmans and D. Depla, "Modeling target erosion during reactive sputtering," *Appl. Surf. Sci.*, vol. 331, pp. 185–192, 2015.

[19] N. D. Madsen *et al.*, "Controlling the deposition rate during target erosion in reactive pulsed DC magnetron sputter deposition of alumina," *Surf. Coatings Technol.*, vol. 206, no. 23, pp. 4850–4854, 2012.

[20] K. Strijckmans *et al.*, "Tutorial: Hysteresis during the reactive magnetron sputtering process," *J. Appl. Phys.*, vol. 124, no. 24, 2018.

[21] Metricon, "MODEL 2010/ M." [Online]. Available: https://www.metricon.com/model-2010-m-overview.

[22] S. Mahieu *et al.*, "Biaxial alignment in sputter deposited thin films," *Thin Solid Films*, vol. 515, no. 4. pp. 1229–1249, 05-Dec-2006.

[23] T. Miyashita and T. Manabe, "Infrared optical fibers," *IEEE J. Quantum Electron.*, vol. 18, no. 10, pp. 1432–1450, 1982.

[24] G. N. West *et al.*, "Low-loss integrated photonics for the blue and ultraviolet regime," *APL Photonics*, vol. 4, no. 2, p. 026101, 2019.

[25] R. G. Hunsperger, *Integrated optics: Theory and technology: Sixth edition*. Springer US, 2009.